arXiv:2505.02703v1 [cs.CV] 5 May 2025

Bare Advanced Demo of IEEEtran.cls for IEEE Computer Society Journals

Zibo Xu, Qiang Li, Weizhi Nie*, Weijie Wang, Anan Liu

Abstract—Medical Visual Question Answering (MedVQA) aims to answer medical questions according to medical images. However, the complexity of medical data leads to confounders that are difficult to observe, so bias between images and questions is inevitable. Such cross-modal bias makes it challenging to infer medically meaningful answers. In this work, we propose a causal inference framework for the MedVQA task, which effectively eliminates the relative confounding effect between the image and the question to ensure the precision of the question-answering (QA) session. We are the first to introduce a novel causal graph structure that represents the interaction between visual and textual elements, explicitly capturing how different questions influence visual features. During optimization, we apply the mutual information to discover spurious correlations and propose a multi-variable resampling front-door adjustment method to eliminate the relative confounding effect, which aims to align features based on their true causal relevance to the question-answering task. In addition, we also introduce a prompt strategy that combines multiple prompt forms to improve the model's ability to understand complex medical data and answer accurately. Extensive experiments on three MedVQA datasets demonstrate that 1) our method significantly improves the accuracy of MedVQA, and 2) our method achieves true causal correlations in the face of complex medical data.

Index Terms—Medical visual question answering, causal inference, front-door adjustment, multi-modal feature alignment, attention mechanism, prompt strategy.

1 Introduction

Medical Visual Question Answering (MedVQA) is an important branch of the Visual Question Answering (VQA) task [1], [2], [3] in the medical field. Its main goal is to accurately answer questions according to medical images, which improves medical diagnosis and treatment efficiency. The rise of this field highlights the potential of artificial intelligence in medical diagnosis [4], [5], [6], providing new possibilities for improving the interpretation of multi-modal medical data and clinical decision-making. Besides, large language models (LLMs) have shown great potential in addressing the MedVQA task by enhancing the understanding of complex medical questions and generating accurate answers [7], [8], [9].

Common VQA tasks [1], [2] are designed to accurately respond to multi-modal inputs comprising images and queries, often focusing on natural images with diverse visual content. These tasks benefit from large-scale datasets and standardized benchmarks that allow models to learn generalizable patterns and associations effectively. However, MedVQA introduces unique challenges compared to common VQA tasks, including the complexity of medical images, which contain specialized and intricate details that require domain-specific knowledge to interpret [10], [11]. Moreover, MedVQA is particularly prone to confounding effects, such as spurious correlations between visual and textual features, which can mislead models and undermine their reliability in clinical applications. Recent MedVQA methods [8], [9], [12] generally rely on large amounts of medical data for pre-training to build visual encoders or language models with medical knowledge. Some of these approaches [8], [12] employ pre-trained encoders to build unique integrated models or introduce a projection module [9] to ensure alignment between medical images and

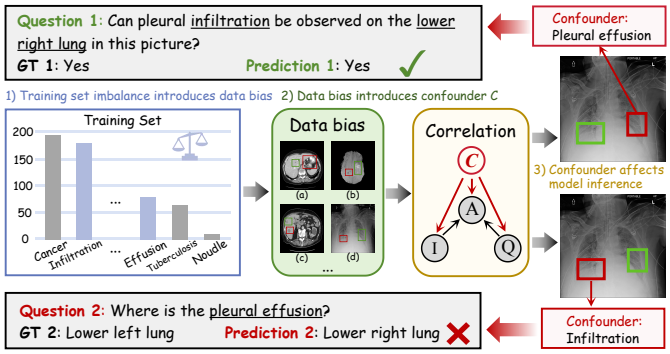

Fig. 1. Illustration of how the confounder C affects model inference. The imbalanced training set leads to data bias, which can manifest in various ways, such as (a) difficulty in learning pathology, (b) statistical association, (c) relativity of confounders, and (d) co-occurrence of multiple pathologies, among others. These biases introduce confounders during inference, creating misleading causal paths. As a result, the model relies on spurious correlations rather than true causal relationships, leading to incorrect predictions.

This work was supported in part by the National Natural Science Foundation of China under Grants U21b2024 and 62272337. (Corresponding author: Weizhi Nie)
Zibo Xu and Qiang Li are with the School of Microelectronics, Tianjin University, Tianjin 300072, China (e-mail: xzb6666@tju.edu.cn, liqiang@tju.edu.cn).
Weizhi Nie and Anan Liu are with the School of Electrical and Information Engineering, Tianjin University, Tianjin 300072, China (e-mail: weizhinie@tju.edu.cn, anan0422@gmail.com).
Weijie Wang is with the Department of Information Engineering and Computer Science, University of Trento, Trento, Italy (e-mail: weijie.wang@unitn.it).
Manuscript received April 19, 2005; revised August 26, 2015.

questions. Although these methods have made remarkable achievements in improving the accuracy of MedVQA, they rely mainly on statistical associations and ignore the potential impact of spurious causation [13] on the inference process.

In the MedVQA field, it's a challenge to understand the rationale behind the answer [9]. Models may fail to identify confounders and spurious associations without considering the effects of multi-modal data bias [14], [15], [16]. In this context, excessive reliance on statistical associations may lead to wrong decisions. When the model answers different medical questions, confounding factors often involve different areas in the image. It means that confounders corresponding to one question may be the real reason for another question, and this relativity is a difficult challenge in MedVQA tasks.

In Fig. 1, the medical training set is highly imbalanced, which introduces data bias and affects model inference. This data bias manifests in multiple ways: (a) difficulty in learning pathology for diseases with fewer samples, (b) statistical associations where certain regions are more frequently linked to specific diseases, (c) relative confounding, where the causal region for one question might act as a confounder for another, and (d) co-occurrence of multiple pathologies, influencing the model's learning preferences. During training, these biases introduce confounders into the causal path, leading to spurious learning pathways and ultimately affecting model predictions.

For instance, when answering whether there is infiltration in the lower right lung, the model provides the correct answer. This is because the question provides sufficient information about both the pathology and location, and due to the larger number of infiltration samples in the training set, the model has learned the relevant features more effectively. However, when the model is asked about the location of pleural effusion, the data bias becomes more evident. The training set contains significantly more cases of infiltration in the lower right lung compared to pleural effusion, and both pathologies share similar visual features. Due to the training data imbalance, the model is exposed to fewer pleural effusion cases, making it harder to learn its distinguishing features. As a result, during inference, the model relies more on frequently seen infiltration patterns, leading to incorrect predictions based on spurious correlations rather than true causal relationships.

The correct use of LLMs in answer generation is also a challenge [3]. When only a single question is provided as textual input, LLMs tend to produce a large number of irrelevant or non-answering statements as answers. This can lead to non-standard answers and a lack of practical reference value. Above all, the issues in the MedVQA task can be summarized as the following two challenges:

1) **How to discover medical multi-modal data bias and eliminate its effects?** The complexity of medical data leads to biases that are difficult to observe and understand [17], [18], [19], [20]. Medical images often contain intricate details that may introduce spurious associations when paired with questions, leading to confounded inference results [13], [21]. These biases are not only challenging to detect but are also variable, with different questions corresponding to different biases within the same medical image. This variability increases the difficulty for models to accurately interpret inputs and deduce correct answers. The presence of confounders can cause the model to focus on irrelevant or misleading associations, ultimately compromising the reliability of the diagnosis or treatment suggestions provided.

2) **How can large language models learn to generate answers with practical reference value?** Large Language Models (LLMs) have been introduced in MedVQA due to their exceptional capabilities in understanding and generating human-like text [7], [8]. However, the application of LLMs in MedVQA is not without challenges. For specific downstream tasks, it is crucial to precisely control the form of the generated text and provide ample guiding information to ensure the answers are accurate and relevant. Without such control, LLMs may generate inaccurate or invalid medical answers, which could mislead patients or medical professionals, potentially causing harm. The complexity of medical terminology and the need for precise, contextually appropriate responses further complicate this task. Ensuring that LLMs can produce answers with practical reference value involves integrating them with specialized modules that can guide their output towards medically valid and useful information.

In order to solve the challenge of data bias in MedVQA, we propose a causal inference framework (CIF). The core idea of CIF is to integrate the structural causal model into the process of visual, textual processing, and answer generation. By eliminating confounding effects, CIF enables the alignment of visual and textual features based on causal relationships, ensuring that the model focuses on causally relevant regions and generates accurate, semantically aligned answers. In this work, we identify invisible confounders in medical data by using mutual information and eliminate the effect of these relative confounders with a multi-variable resampling front-door adjustment method. Besides, we introduce a prompt module that generates a series of prompt texts for each set of data to enhance the model's understanding of the QA pairs and images. This improves the model's ability to generate meaningful answers.

Our contributions can be summarized as:

- We propose a novel multi-variable correlated causal inference framework (CIF), which first considers the relative biases caused by data bias in medical VQA. We apply the multi-variable resampling front-door adjustment, which not only considers the potential differences between the multi-modal data, but also effectively eliminates the interference of confounding factors.
- We propose a prompt strategy that integrates a prompt module into the MedVQA backbone. This strategy guides the language model to generate accurate and standardized answers by providing auxiliary information, thus enhancing the model's ability to understand and respond to questions despite the complexity of aligning different modalities.
- The effectiveness of our method has been strongly validated on five MedVQA datasets. These validations demonstrate the robustness and generalizability of our approach, confirming its capability to handle diverse MedVQA scenarios.

2 Related Work

2.1 Causal Inference

The purpose of causal inference [13] is to pursue causal effects and eliminate false biases [22]. In recent years, causal models have gained widespread acclaim in computer vision tasks for their superior inference abilities [21], [23], [24], [25], [26]. Yue et al. [27] adjust the deletion bias by backdoor adjustment and made some simple assumptions. Li et al. [25] propose a causal Markov model based on the variational autoencoder (VAE) structure to decompose disease-related variables. Yang et al. [28] propose causal attention (CATT) based on front-door adjustment, enhancing the quality of the attention mechanism. Zhang et al. [5], [6] classify medical images through a causal perspective and utilize instrumental variables to reduce potential ambiguities in medical images. Zang et al. [29] reexamine causal effects in multi-modal data and introduces a causal prediction architecture. However, the current causal models mainly focus on finding confounders and reducing their effects [5], but neglect the relativity of confounders. This can lead to poor generalization when dealing with complex cross-modal tasks.

2.2 Medical Visual Question Answering

The traditional MedVQA approach [4], [30], [31], [32] aims to apply the best VQA models to the medical field; they use medical data to fine-tune VGG [33] or ResNet [34] for visual feature extraction. Nguyen et al. [11] explore the use of the unsupervised Denoising Auto-Encoder (DAE) [35] and the supervised Meta-Learning [36] for visual feature extraction. Based on [11], Zhan et al. [10] further enhance the reasoning ability of the multi-modal feature fusion module. Liu et al. [37] propose a two-stage pre-training framework to tackle the challenge of data scarcity. Chen et al. [38] acquire cross-modal knowledge by using random masks to reconstruct missing pixels and markers in images and text. With the popularity of LLMs, Lin et al. [12], Wu et al. [8] using large amounts of medical data to pre-train models, Li et al. [7] propose a model with powerful conversational capabilities and highlight that the lack of deep reasoning is a common shortcoming of existing approaches. In addition, Zhang et al. [9] collect an extensive data set and design a projection module to align visual and textual attributes. Huang et al. [39] propose a dual-attention learning network for MedVQA. However, the above methods effectively transform the model into a medical knowledge base, where the QA process involves selecting the best answers from a wide but limited pool of answers. Such methods ignore the relativity of confounders in medical data and the spurious associations caused by confounders.

2.3 Causal Inference in MedVQA

Recent studies have explored causal inference techniques to mitigate biases in MedVQA, aiming to improve model robustness and interpretability. Various counterfactual-based approaches have been proposed to address different types of biases. Zhan et al. [40] propose a counterfactual debiasing framework to mitigate language bias in MedVQA through dual interventions. Ye et al. [41] propose a causal framework to mitigate modality preference bias in MedVQA by counterfactual inference. The method eliminates spurious question-answer correlations through causal path decomposition, subtracting the bias effect in scenarios where medical images are absent. Cai et al. [42] propose a counterfactual causal-intervention strategy for MedVQA, leveraging layer-wise relevance propagation to generate interpretable saliency maps and mitigate language bias. While these methods mitigate biases through counterfactual inference, they mainly focus on direct associations. However, MedVQA involves complex interactions where indirect causal effects also contribute to biases.

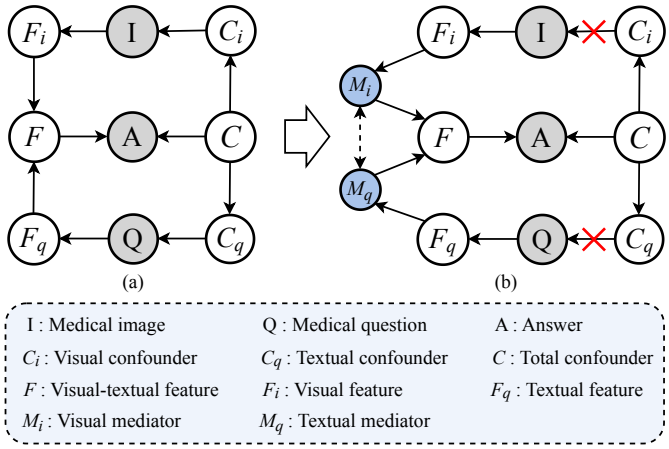

Fig. 2. Causal directed acyclic graph of MedVQA, gray variables are observed data, and blue variables are mediators. **(a)** Important variables in MedVQA and their associations. **(b)** We apply the front-door adjustment by introducing two mediators to deal with the invisible confounders. This reveals the true causal relationship between $\{I, Q\}$ and A. The dashed line between the two mediators reflects the relative confounders considering the interaction between the two modalities.

3 Methodology

3.1 Causal Analysis of MedVQA

We use the structural causal model [13], [43] to represent the causal relationships in the MedVQA task. Each node represents a key variable, and the connecting lines represent the causal relationship between the variables, as shown in the causal graph Fig. 2(a).

$I \leftarrow C_i \leftarrow C \rightarrow A$ and $Q \leftarrow C_q \leftarrow C \rightarrow A$ are the backdoor paths of $\{I, Q\} \rightarrow F \rightarrow A$ respectively, where total confounders C consist of visual confounders C_i and textual confounders C_q. C arises from biases in medical multi-modal data, leading to spurious associations between $\{I, Q\}$ and A. For example, a spurious, strong correlation may appear between a medical question and a pathology in an image or between two pathologies in an image. When answering according to I and Q, if the model only learns the statistical association $P(A|I, Q)$, it will ignore the influence of spurious associations raised by confounders C, leading to generating incorrect answers.

$I \rightarrow F_i \rightarrow F \leftarrow F_q \leftarrow Q$ represents the extraction and fusion process of medical image features and textual features. In this process, I and Q are converted into features F_i and F_q by feature extraction modules. Subsequently, F_i and

F_q fuse into the multi-modal joint feature F, and the efficient capture and integration of F form the basis of true causality. However, due to the existence of the backdoor paths, F extracted by learning the statistical association $P(A|I,Q)$ is bound to be affected by confounders C, resulting in some confounding features and false causal associations in F_i and F_q.

$F \rightarrow A$ represents a direct connection between the fusion feature and the answer. Ideally, this connection should be independent of the variable C, and the path should be the only source from which the answer is generated.

Taking the example in Fig. 1, where $P(c =$ "infiltration" $|I =$ "abnormal area", $Q =$ "right") is much larger than $P(c =$ "effusion" $|I =$ "abnormal area", $Q =$ "right"), so $P(A|I,Q,c =$ "infiltration") plays a more important role than $P(A|I,Q,c =$ "effusion") when calculating $P(A|I,Q)$. This leads the model to over-rely on the spurious correlation between the "right" lung and "infiltration" rather than correctly distinguishing between pathologies. The causal inference intervenes by breaking these spurious correlations, ensuring that $P(A|do(I,Q))$ is computed based on causal relationships rather than statistical associations. To achieve this, we model the conditional probability by explicitly integrating causal paths within the network design. Specifically, the structural causal model provides a mechanism to estimate and adjust for the influence of confounders, aligning $P(A|do(I,Q))$ with its true causal components.

In subsequent sections, we demonstrate how the probability is implemented within the network through specific modules, where the causal adjustment process is implemented as part of the alignment of multi-modal features.

3.2 Causal Inference Techniques in MedVQA

Ideally, we can employ causal analysis and causal inference to intervene with $\{I,Q\}$, ensuring that the model avoids erroneously capturing spurious correlations $\{I,Q\} \leftarrow C \rightarrow A$ introduced by confounders C, and instead accurately captures real causal structure $\{I,Q\} \rightarrow A$ [43].

3.2.1 Front-door adjustment

Confounders in medical multi-modal data are often complex and unobserved. In this case, front-door adjustment is a feasible method of causal intervention [13]. The core idea of causal intervention is to cut off the backdoor path to $\{I,Q\}$ by $do(I,Q)$, as shown in Fig. 2(b). However, since C_i and C_q are often unobserved, we introduce two mediators, m_i and m_q to implement the process of removing confounders. In MedVQA tasks, the data of the two modalities are often closely related, so m_i and m_q are not actually independent. We combine Fig. 2(b) with the front-door adjustment:

$$\begin{aligned} &P(A|do(I,Q)) \\ &= \sum_m P(A|do(M=m))P(M=m|do(I,Q)) \\ &= \sum_{m\in\mathcal{M}} \sum_{i\in I} \sum_{q\in Q} P(A|m,i,q)P(i,q)P(m|I,Q) \\ &= \sum_{m\in\mathcal{M}} P(m|I,Q) \sum_{i\in I} \sum_{q\in Q} P(A|m,i,q)P(i,q), \end{aligned} \tag{1}$$

where m=$\{m_i^1, \cdots, m_i^k, m_q^1, \cdots, m_q^n\}$ is the set of mediators, k and n are related to images and questions, respectively. i and q are approximately sampled from $\{I,Q\}$ at the feature level [44]. $P(A|m,i,q)$ represents the combined influence of preprocessed medical data and mediators on answers.

Since the answer generation part of the MedVQA task is essentially to select the best answer from a large corpus, $P(A|m,i,q)$ can be approximated as a network g(·) followed by softmax [28]:

$$P(A|m,i,q) = \text{Softmax}(g(m,i,q)). \tag{2}$$

Theoretically, Eq. 1 requires sampling all medical data and corresponding mediators. To simplify this process, we use the Normalized Weighted Geometric Mean (NWGM) [44] to further approximate:

$$\begin{aligned} &WGM(f(x)) = \prod_x f(x)^{P(x)} = \prod_x exp[g(x)]^{P(x)} \\ &= exp[\sum_x g(x)P(x)] = exp[\mathbb{E}_x[g(x)]] \approx \mathbb{E}_x[f(x)], \\ &N(f(x)) = \frac{\prod_x exp(g(x))^{p(x)}}{\sum_j \prod_x exp(g(x))^{p(x)}} = \text{Softmax}(\mathbb{E}_x[g(x)]). \end{aligned} \tag{3}$$

where function W denotes Weighted Geometric Mean and N denotes NWGM, $f(x) = exp[g(x)]$. Then the sampling process can be expressed as:

$$\begin{aligned} &\sum_{i\in I} \sum_{q\in Q} P(A|m,i,q)P(i,q) = \mathbb{E}_{i,q}\text{Softmax}(g(m,i,q)) \\ &= \text{Softmax}(g(m,\mathbb{E}_{i,q}(i,q))) = \text{Softmax}(g(m,\boldsymbol{i},\boldsymbol{q})), \end{aligned} \tag{4}$$

where $\mathbb{E}_{i,q}$ denotes the expectation function, $\boldsymbol{i}$, $\boldsymbol{q}$ denote the estimations of i, q. Then $P(A|do(I,Q))$ can be obtained as:

$$\begin{aligned} &P(A|do(I,Q)) = \sum_{m\in\mathcal{M}_i} \text{Softmax}(g(m,\boldsymbol{i},\boldsymbol{q}))P(m|I,Q) \\ &= \text{Softmax}[G(\boldsymbol{m},\boldsymbol{i},\boldsymbol{q})] = \text{Softmax}[G(\boldsymbol{m_i},\boldsymbol{m_q},\boldsymbol{i},\boldsymbol{q})], \end{aligned} \tag{5}$$

where $G(\cdot)$ represents the overall causal inference network, and $\boldsymbol{m}$ denotes the estimations of m.

We approximate causal intervention $P(A|do(I,Q))$ as the process of combining medical visual and textual features with their corresponding mediators. We introduce mutual information to quantify the correlation between images and questions, ensuring that the sampling processes of $\boldsymbol{m_i}$, $\boldsymbol{m_q}$ are based on the true correlations between the two modalities. $\boldsymbol{i}$ and $\boldsymbol{q}$ are essentially extracted features f_i and f_q, presenting in F_i and F_q in the causal graph Fig. 2. $\boldsymbol{m_i}$, $\boldsymbol{m_q}$ are calculated by mediator integrators. The detailed deconfounding process is shown in Fig. 4.

Through the steps above, we have expressed the causal effect as a combination of image and question features. However, to address the potential confounders in both image and text, we introduce two specialized sub-networks:

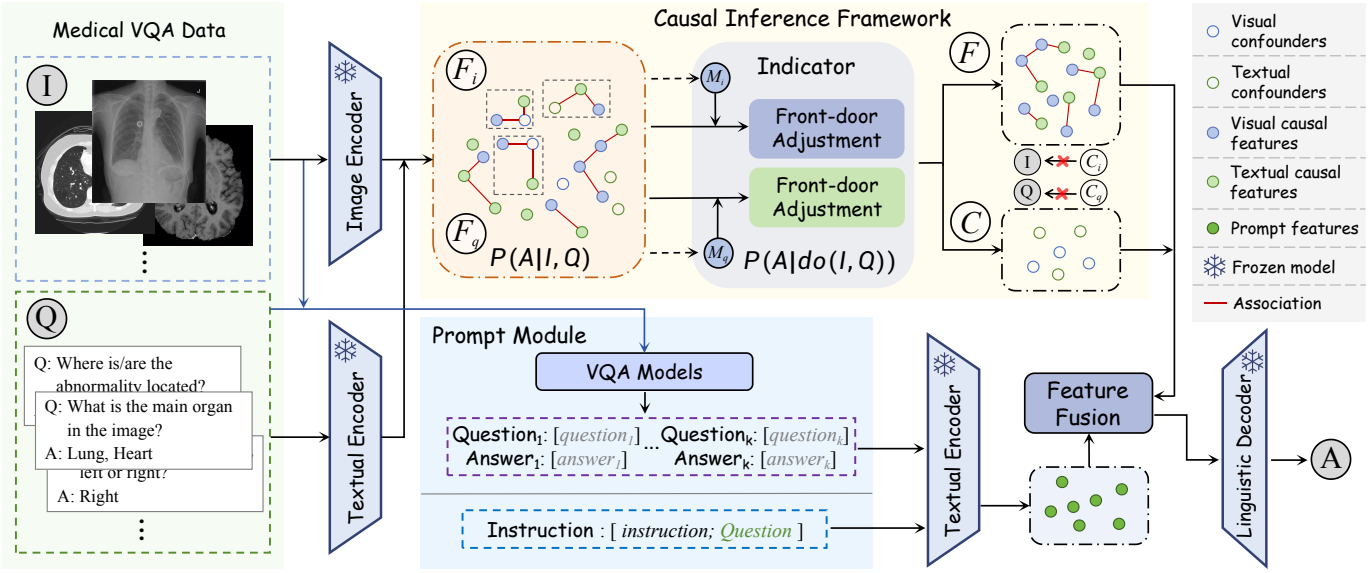

Fig. 3. Overview of our method. There are causal features, confounding features, and their spurious associations in the feature space. We introduce an indicator module to obtain true causal features in MedVQA data, where we use mutual information to adjust the factors that may lead to spurious associations when learning mediators. For the features of two modalities, we use a multi-variable resampling front-door adjustment method to separate causation and confounding factors. The prompt module receives a variety of inputs, including instruction, questions, and a new set of QA pairs generated from each original data, which are then fed into the pre-trained linguistic decoder as an overall prompt for answering.

the visual de-confounding network and the textual de-confounding network:

$$P(A|do(I,Q)) \propto \text{Softmax}\left(\sum_{m_i \in \mathcal{M}_i} \sum_{m_q \in \mathcal{M}_q} Y(m_i, f_i, f_q) \cdot H(m_q, f_i, f_q)\right), \tag{6}$$

where the functions $Y(m_i, f_i, f_q)$ and $H(m_q, f_i, f_q)$ represent the interactions between image and question features. In Eq. 6, the interactions between features is jointly modeled through the de-confounding networks Y and H, effectively removing confounders in both image and question, and enabling an accurate estimation of the causal effect.

In the next section, we will provide a detailed explanation of how to implement these two de-confounding networks, particularly how they utilize attention mechanisms and feature interactions to eliminate confounders, improving the robustness and performance of the model.

3.2.2 Implement method

Given the medical image $i \in \mathbb{R}^{H \times W \times 3}$ as input, we use the pre-trained image encoder Clip ViT-B/16 [45] to extract the feature $f_i \in \mathbb{R}^{h \times w \times d}$, where $H \times W$ and $h \times w$ represent the height and width of the medical image and the feature map, respectively, and d represents the hidden dimension of the network. Medical questions involve semantic content such as image types, organs, and pathology, while answers are often short, typically consisting of only one to four words [30], [46], [47]. We use a hierarchical semantic parser [43] to transform medical questions into image-based markers, extract semantic associations from the medical knowledge base, and decompose the questions into different forms. The parsed outputs are then processed by the frozen LLaMA encoder, which encodes these structured semantic representations into high-dimensional embeddings. This hierarchical parsing and encoding pipeline ensures that the questions are semantically enriched and properly aligned with the model's visual features, facilitating causal reasoning and accurate cross-modal alignment. The two feature extraction processes are as follows:

$$f_i = \Phi_{ie}(i, \Theta_i), \quad f_q = \Phi_{qe}(q, \Theta_q), \tag{7}$$

where Φ_{ie}, Φ_{qe} represent the pre-trained image encoder and the textual encoder, and Θ_i and Θ_q represent their corresponding parameters.

The Feature Mapping Module (FMM) is developed to extract global features f_{ig} and local features f_{il} from medical images, enabling complementary representations for downstream tasks. For global sampling, FMM employs a Down-Sampling Transformer block that aggregates visual tokens to retain the overall structure and spatial layout of the image. This captures macroscopic details, such as the relative positioning and contours of organs, providing crucial contextual information for reasoning. For local sampling, inspired by attention mechanisms, the FMM leverages accumulated attention maps to identify and extract the top k tokens that correspond to regions of interest, such as lesions or abnormalities. For each attention head, k=8 tokens are selected, providing granular and contextually significant details that align with the limited image diversity. This ensures that fine-grained details essential for precise question answering are effectively captured. The combination of these two sampling strategies enhances the model's capacity to align global context with local precision, which is particularly vital for the complex reasoning required in MedVQA tasks.

In MedVQA, the model needs to establish the correct connection between the medical image and the question. In this case, we use a feature fusion module to generate the

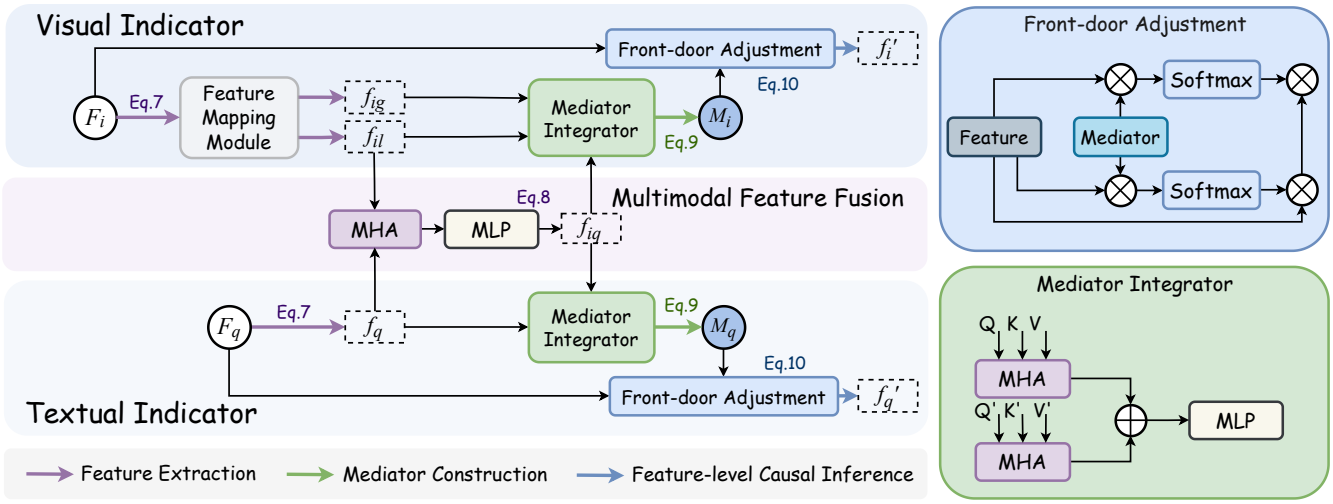

Fig. 4. Overview of indicator structure. The indicator structure consists of a visual indicator, a text indicator, and a multi-modal feature fusion module. This structure generates two mediators, which are combined with F_i and F_q to obtain true causal features by front-door adjustment.

cross-modal interaction features f_{iq}:

$$f_{iq} = MLP(MHA(f_{il}, f_q, f_q)), \tag{8}$$

MHA and multi-layer perceptron (MLP) constitute feature fusion modules. Here, f_{il} represents the local visual feature extracted from the image, while f_q is the textual feature derived from the question. This structure ensures that local image features remain central, while question features are incorporated to guide attention and align the semantic meaning across modalities. According to Fig. 4, in the indicator structure, we use front-door adjustment for visual features and linguistic features, respectively. Considering the interaction between the two modalities and the relativity of confounders, we use mutual information and multivariate resampling methods to sample the two mediators:

$$\begin{aligned} \boldsymbol{m_i} &= MLP(MHA(f_{il}, f_{ig}, f_{ig}), MHA(f_{il}, f_{iq}, f_{iq})), \\ \boldsymbol{m_q} &= MLP(MHA(f_q, f_q, f_q), MHA(f_{iq}, f_q, f_q)), \end{aligned} \tag{9}$$

where $\boldsymbol{m_i}$ and $\boldsymbol{m_q}$ are the visual and textual mediators, respectively. The rationale for these designs is as follows. For $\boldsymbol{m_i}$, $MHA(f_{il}, f_{ig}, f_{ig})$ captures the relationship between local features f_{il} and global features f_{ig}, while $MHA(f_{il}, f_{iq}, f_{iq})$ integrates question-specific focus into the visual feature representation. This combination enables the model to account for both overall structural information and localized details relevant to the question. For $\boldsymbol{m_q}$, $MHA(f_q, f_q, f_q)$ emphasizes linguistic coherence within the question text, while $MHA(f_{iq}, f_q, f_q)$ incorporates cross-modal semantic alignment between textual and visual features. These mediator designs are carefully chosen to balance intra-modal dependencies and cross-modal interactions, providing robust causal feature adjustments.

The extracted multi-modal feature f_{iq} contributes to the interaction between the two modalities when extracting $\boldsymbol{m_i}$ and $\boldsymbol{m_q}$ in Eq. 9, and helps the model focus on the confounding areas specified by the question. $\boldsymbol{m_i}$ reveals the relationship between the local features, global features, and fusion features of medical images. $\boldsymbol{m_q}$ reveals the associations between different parts of the medical question text and the semantic connections between fusion features and textual features.

Areas of interference in the same medical image vary with different questions. This means that word features affect areas of concern for visual features through cross-attention. Considering this relativity of confounders, we resample the mediators to ensure that we can discover and adjust for the proprietary confounder for each question. This dynamic adjustment ensures that $\boldsymbol{m_i}$ and $\boldsymbol{m_q}$ capture the essential causal relationships between modalities while effectively mitigating confounding effects. By introducing the front-door adjustment module, the entire process of causal inference and the processes of deconfounding the causal and confounding factors of multi-modal medical data can be represented as:

$$\begin{aligned} P(A|do(I,Q)) &= \text{Softmax}[\boldsymbol{g}(Y(f_i, \boldsymbol{m_i}), H(f_q, \boldsymbol{m_q}))], \\ f_i^{'} &= Y(f_i, \boldsymbol{m_i}), f_q^{'} = H(f_q, \boldsymbol{m_q}), \end{aligned} \tag{10}$$

where $\boldsymbol{g}(\cdot)$ represents a feature fusion network, Y, H represent the visual front-door adjustment and the textual front-door adjustment, $f_i^{'}$, $f_q^{'}$ are visual causal features, and textual causal features, respectively.

3.3 Prompt Module

In MedVQA, random outputs generated by LLMs may result in only a small fraction of the content matching the ground truth. In order to obtain medically meaningful answers, we design a Prompt Module (PM). PM is designed for MedVQA, which poses greater challenges compared to natural images due to the presence of complex structures. Our approach involves leveraging pre-trained visual and linguistic backbones to effectively generate QA pairs, and we design different templates for reference of LLMs. In essence, we position PM as a pivotal component complementing CIF, enhancing the effectiveness of LLMs in generating answers by incorporating causal features.

The Prompt Module (PM) is seamlessly integrated into the MedVQA framework to enhance the reasoning capabilities of LLMs by embedding structured prompts into

the QA stage. Specifically, we employ two distinct types of instructions to serve different purposes. For QA pairs generation, $\text{Instructions}_{\text{gen}}$ guide the generation of QA pairs based on medical images, ensuring alignment with clinical reasoning. These predefined instructions are critical for creating meaningful QA pairs and are detailed in Table 1. For task introduction, $\text{Instructions}_{\text{task}}$ provide context to the LLM for the final output generation. For example, "You are a doctor, please answer the question based on the medical image and QA pairs." While $\text{Instructions}_{\text{task}}$ is not essential to model performance, it helps standardize interactions with the LLM by briefly introducing the task requirements.

Besides, we precede the input question with a series of generated QA pairs $\{Q_n; [Question], A_n : [Answer]\}$ for each set of Image-QA pairs, acting as exemplars to guide the model. These prompts serve as caption-like guidance, helping the model focus on causal patterns rather than relying solely on textual cues. The specific template is shown in Table 1.

The generation process for the prompts is straightforward and efficient. Using the pre-trained visual and linguistic backbones (CLIP ViT-B/16 and LLaMA), the model directly infers QA pairs from each original data point in the dataset. The generated QA pairs take the form, representing meaningful examples that align with the underlying medical context. The prompt structure integrates these generated QA pairs along with task instructions and the current question, formatted as $\{Instructions_{task}$,$[QA]_n$,$Question$:$[Question]$,A :$\}$, $n \in [1, 3]$. For the prompt text, we use the same feature extraction method as for medical questions.

TABLE 1
Templates for different types of questions used to generate QA pairs.

Type	Template of QA pairs
QA Pairs	
What	What $[organ(s)/disease(s)]$ is/are in the image?
Which	Which $[disease(s)/organ(s)]$ is/are in the image?
Where	Where is/are the $[abnormality/organ(s)]$ located?
Is	Is this a/an $[imaging\ techniques/organ]$?
Does	Does the image contain $[organ/abnormality]$?
Which	Which side is $[organ/abnormality]$ in the image?
Instructions	Describe the following medical image in detail.
	Answer the question based on the medical image.
	Provide a detailed analysis of the medical image.
	Analyze the medical image and describe any abnormalities.
	Based on the image, provide a differential diagnosis.

3.4 Training Strategy

For closed questions and open-ended questions, we design different loss functions, for closed questions, we apply supervised loss in a cross-entropy format:

$$\mathcal{L}_c = -\frac{1}{|\mathbf{T}|}\sum_{\boldsymbol{t}\in\mathbf{T}} \boldsymbol{a_t}^{\top} log(\mathbf{V}(i, q)), \tag{11}$$

where $\boldsymbol{a_t}$ represents the ground-truth answer, $\mathbf{T}$ is the training data, $\mathbf{V}(\cdot)$ denotes our proposed framework.

For open-ended questions, the loss function is:

$$\mathcal{L}_o = -\sum_{\boldsymbol{n}=1}^{\mathbf{N}} log\mathbf{p}(\boldsymbol{a_n}|i, q, \boldsymbol{p_t}, \boldsymbol{a_{1:n-1}}; \Theta_o), \tag{12}$$

where $\mathbf{N}$ is the length of the ground-truth, $\boldsymbol{a_{1:n-1}}$ denotes previous tokens, Θ_o denotes the parameter of the model, and $\boldsymbol{p_t}$ is the prompt text. Eq. 12 allows the model to generate answers based on multi-modal inputs and partial outputs, which is more efficient than categorizing in candidate answer sets. To make the predictions of original features and causal features consistent and highlight the true causal effect, we design a loss function:

$$\mathcal{L}_{cau} = \mathbf{KL}(\mathbf{V}(f_i^{'}, f_q^{'}), \mathbf{V}(f_i, f_q)), \tag{13}$$

where $\mathbf{KL}$ is the KL-divergence. Finally, the overall learning objectives for two forms of questions are:

$$\mathcal{L}_{closed} = \mathcal{L}_c + \mathcal{L}_{cau}, \mathcal{L}_{open} = \mathcal{L}_o + \mathcal{L}_{cau}. \tag{14}$$

For datasets such as ProbMed and PMC-VQA, where questions are not explicitly categorized into closed-ended and open-ended forms, we adopt the loss function designed for open-ended questions. This choice is motivated by the fact that answers in these datasets tend to be more diverse and detailed, making the open-ended loss function more suitable.

4 Experiment

4.1 Datasets

VQA-RAD [30] is a dataset specifically designed for radiology, consisting of 315 images and 3,515 questions with 517 possible answers. The dataset includes 3,064 tasks for training and 451 tasks for testing. All questions are concise, typically ranging from 5 to 7 words, while the answers are even shorter, averaging about 1.6 words each.

SLAKE [46] is an English-Chinese bilingual MedVQA dataset consisting of 642 images and 14k QA pairs, covering 12 diseases and 39 systemic organs. Diseases mainly include tumors and chest diseases, and the images mainly include the head, chest, abdomen, pelvic cavity, and other body parts. We follow the original dataset splitting, where 4,919 tasks about 450 images are used for training, 1,053 tasks about 96 images for validation, and 1,061 tasks about 96 images for testing.

PathVQA [47] is a pathological image dataset containing 4998 pathological images, and 32,799 QA pairs. Each image is accompanied by multiple questions covering various aspects such as location, shape, color, appearance, etc. In the official dataset split, the training set, validation set and test set contain 19,755, 6,279 and 6,761 QA pairs, respectively.

PMC-VQA [50] is a large-scale MedVQA dataset of 227,000 QA pairs that cover 149,000 images, covering multiple modes of medical imaging and types of diseases. It was constructed to support and facilitate the development of MedVQA models, especially in generative QA tasks, capable of addressing diverse questions that arise in clinical practice. All questions are multiple-choice. In the official dataset split, the training set and test set 82 % and 18%.

ProbMed [51] is a probe evaluation dataset for medical diagnosis, containing 6,303 images and 57,132 QA pairs covering a wide range of image modes and organs. The dataset requires the model to reason across multiple diagnostic dimensions, including modal recognition, organ recognition, clinical findings, anomalies, and location reasoning. Since the dataset was not explicitly divided officially,

TABLE 2
Comparison of accuracy with state-of-the-art methods on three MedVQA datasets. Questions are divided into open and closed questions. Also, "Overall" indicates the overall accuracy over each entire dataset. The second-best results are underlined.

Method	VQA-RAD			SLAKE			PathVQA		
	Open	Closed	Overall	Open	Closed	Overall	Open	Closed	Overall
MEVF-BAN [11]	49.2	77.2	66.1	77.8	79.8	78.6	8.1	81.4	44.8
CPRD-BAN [37]	52.5	77.9	67.8	79.5	83.4	81.1	-	-	-
M3AE [38]	67.2	83.5	77.0	80.3	87.8	83.3	-	-	-
PMC-CLIP [12]	67.0	84.0	77.6	81.9	88.0	84.3	-	-	-
CLIP-ViT [48]	-	-	-	84.3	82.1	83.3	40.0	87.0	63.6
M2I2 [49]	66.5	83.5	76.8	74.7	91.1	81.2	36.3	88.0	62.2
LLaVA-Med [7]	64.4	82.0	74.9	84.7	83.2	84.1	38.9	**91.7**	65.3
MedVInT-TE [9]	69.3	84.2	78.2	88.2	87.7	88.0	-	-	-
MedVInT-TD [9]	73.7	86.8	81.6	84.5	86.3	85.2	-	-	-
Ours (7B)	74.3	87.1	82.0	90.1	90.4	90.2	40.4	87.9	64.2
Ours (13B)	**76.0**	**87.9**	**83.1**	**90.5**	**91.8**	**91.0**	**41.4**	91.5	**66.5**

we randomly divided it into the training and test sets at a ratio of 4:1.

4.2 Implementation details

Experimental Setup. We adopt the open-sourced ViT-B/16 from CLIP [45] as our visual backbone and LLaMA [8] as the large language model (LLM) for our MedVQA tasks. Both the visual backbone and the LLM remain frozen during training to leverage their pre-trained capabilities without additional fine-tuning. For the LLM, we select models with 7B and 13B parameters for evaluation. The input image resolution for the visual backbone is set to 224×224 pixels. Since the image types and QA pairs among five datasets are relatively similar, we use the same feature extraction strategy. To train our causal inference framework (CIF), we employ the AdamW optimizer with a weight decay of 0.05. The initial learning rate is set to 1e-4 , which decays to 1e-7 following a cosine annealing schedule. The model is trained for 100 epochs with a batch size of 16. All models are implemented in PyTorch and trained on 2 NVIDIA GTX 4090 GPUs.

Data Preprocessing. To support feature extraction and multimodal integration, we use CLIP's ViT-B/16 as the visual backbone and LLaMA's encoder as the language backbone. Both backbones remain frozen during training to preserve their pre-trained knowledge. Visual tokens are generated from input images resized to a resolution of 224×224, where FMM processes them into f_{ig} and f_{il} as described above. The f_{ig} representation provides a holistic understanding of the image, while f_{il} captures fine-grained, region-specific information, such as anomalies or detailed structures. These embeddings are critical for datasets like VQA-RAD and PathVQA, where precise and diverse visual reasoning is required.

On the textual side, the LLaMA encoder is employed to generate text embeddings from input medical questions. The encoder maps questions into a semantic space that aligns with the extracted visual features, facilitating effective multimodal fusion. These embeddings, together with f_{ig} and f_{il}, form the input to the causal inference framework, enabling robust reasoning across diverse datasets, including PMC-VQA with its large-scale multimodal data and SLAKE, which requires reasoning across multiple organs and diseases.

TABLE 3
Distribution and accuracy of closed questions in the SLAKE dataset, where "Else" includes those posed with "Is/Are", "Are/Is", and "Where".

	Does	Is	Which	Are	Do	Can	Else
Train	904	492	242	109	88	67	41
Val	170	115	55	19	29	20	14
Test	172	119	54	21	25	18	7
Total	1246	726	351	149	142	105	62
w/o CIF	**87.2**	**82.4**	**74.1**	**76.2**	**84.0**	**77.8**	**71.4**
w/ CIF	**93.0**	**89.1**	**83.3**	**85.7**	**92.0**	**88.9**	**85.7**

4.3 Main Results

4.3.1 Results on VQA-RAD

As shown in Table 2, we achieve the best performance on both open and closed questions by using a language backbone LLaMA with different parameters, 7B and 13B. In particular, we achieve significantly improved performance when using the 13B backbone. Specifically, we achieve a 2.3% accuracy improvement for open questions and a 1.1% accuracy improvement for closed questions. Combining the overall VQA-RAD dataset, our method outperforms the current state-of-the-art (SOTA) approach by 1.5%.

4.3.2 Results on SLAKE

Compared to all existing MedVQA methods, our method demonstrates the best performance on almost all types of questions. Notably, when using LLaMA-13B as the language backbone, we achieve the highest accuracy across the overall dataset. Our method exhibits a 2.3% accuracy improvement for open-ended questions compared to the current SOTA. While our accuracy in closed questions is slightly lower than the M2I2 method, our overall dataset performance surpasses the second-place method by 2.3%.

We also conduct statistics on the distribution and accuracy of different types of questions in the SLAKE dataset, and the specific results are shown in Table 3 and Table 4. The introduction of the CIF framework brings consistent improvements across all question types in the SLAKE

TABLE 4
Distribution and accuracy of open questions in the SLAKE dataset, where "Else" includes those posed with "In what" and "Does".

	What	Which	Where	How	Else
Train	1640	577	389	342	28
Val	340	127	72	86	6
Test	339	125	89	84	8
Total	2319	829	550	512	42
w/o CIF	**81.7**	**80.8**	**85.4**	**71.4**	**50.0**
w/ CIF	**91.4**	**90.4**	**93.3**	**85.7**	**75.0**

dataset. Specifically, CIF effectively reduces the impact of spurious correlations by aligning visual and textual elements under a causal reasoning framework. This alignment leads to significant accuracy gains, especially for sparse and complex question types such as "Else" (+14.3% for closed questions, +25.0% for open questions) and "How" (+14.3% for open questions). For common question types like "Does" and "Is", where the baseline performance is already high, CIF further enhances accuracy by approximately 5-7%, demonstrating its ability to refine model reasoning even for simpler tasks. These results indicate that CIF not only improves the robustness of the model across diverse question distributions but also enhances its ability to handle complex reasoning and semantic alignment challenges in the MedVQA task.

However, for questions posed in "How" (most of which included "How to" and "How many"), the accuracy was relatively low, suggesting that the model still faces challenges in image segmentation and disease inference.

4.3.3 Results on PathVQA

According to our evaluation results on the PathVQA dataset in Table 2, our approach outperforms current SOTA by 1.4% in open questions and 1.2% in the overall dataset. Notably, the answers to the open-ended questions in the PathVQA dataset are more complex than those in SLAKE and VQA-RAD, which requires models to have a stronger ability to reason and answer creatively, and our model has clear advantages in this respect. Our approach aims to generate answers rather than categorize them from a collection of answers, which enables better performance in terms of open-ended questions.

4.4 Ablation Study

4.4.1 Module analysis

As shown in Table 5, we verify the validity of CIF and PM on two language backbones (7B, 13B).

Effectiveness of CIF. When using only CIF, we observe substantial improvements in accuracy across all datasets and question types, particularly for datasets with complex reasoning tasks and high-confounding features such as PathVQA and ProbMed. CIF improves overall accuracy by up to 9.0% (from 51.1% to 60.1%) on PathVQA (7B) and by 13.3% (from 53.0% to 66.3%) on ProbMed (7B). These results indicate that CIF effectively mitigates the impact of spurious correlations, allowing the model to focus on causal relationships between visual inputs, questions, and answers. CIF also shows consistent improvements in datasets like SLAKE and VQA-RAD, which include a mix of open and closed questions. For example, in SLAKE, CIF improves the overall accuracy from 79.9% to 85.5% (7B) and from 80.6% to 86.5% (13B), demonstrating its ability to generalize across different question types. The significant improvements for open questions in SLAKE and PathVQA further highlight CIF's capability to address tasks requiring complex reasoning by aligning key visual and textual elements under causal relationships.

Effectiveness of PM. The prompt module (PM) also leads to noticeable improvements, particularly in datasets where the complexity of medical questions and textual context poses challenges for large language models (LLMs). PM enhances the model's understanding of complex medical questions by providing structured guidance through prompts, which dynamically adapt to the context of each question. For example, on ProbMed, PM increases overall accuracy from 53.0% to 57.9% (7B) and from 54.0% to 59.1% (13B). Similarly, in PathVQA, PM improves the overall accuracy by 1.9% (from 51.1% to 53.0%) for 7B and by 2.3% (from 51.9% to 54.2%) for 13B. The impact of PM is particularly pronounced in datasets with diverse question types, such as SLAKE and PMC-VQA, where it facilitates better alignment between textual inputs and the causal features extracted by the model. For example, in SLAKE, PM increases overall accuracy from 79.9% to 81.2% (7B) and from 80.6% to 81.9% (13B), demonstrating its effectiveness in improving the model's ability to interpret nuanced medical concepts. On PMC-VQA, PM increases accuracy from 36.0% to 38.5% (7B) and from 36.6% to 40.8% (13B). On VQA-RAD, PM provides a modest 0.3% overall accuracy gain (from 78.2% to 78.5% for 7B). This limited impact is due to VQA-RAD's relatively structured question-answer format, where most questions adhere to consistent patterns, reducing the need for additional prompt-based guidance.

Combined Effect of CIF and PM. The best performance is achieved when CIF and PM are used together, resulting in the highest accuracy across all datasets. On ProbMed, the combined approach achieves an overall accuracy of 69.4% (7B) and 70.7% (13B), representing improvements of 16.4% and 16.7%, respectively, compared to the baseline without CIF and PM. On PathVQA, accuracy increases to 64.2% (7B) and 66.5% (13B), highlighting the importance of combining causal alignment (CIF) with the semantic guidance provided by PM. On PMC-VQA, while the 0.4% improvement for 7B may seem modest, it remains meaningful given the dataset's large scale and diversity. With 227K QA pairs, even a small percentage gain translates to tangible improvements across hundreds of cases. This complementary effect can be attributed to the distinct roles of CIF and PM in the MedVQA pipeline: CIF eliminates confounders by aligning visual and textual features under causal relationships, reducing the model's reliance on spurious correlations. This ensures that the features extracted by the model are relevant and task-specific. PM further enhances the utilization of these causal features by providing question-specific guidance, allowing the LLMs to focus on contextually important information. While CIF ensures that the extracted features are causally valid, PM makes these features more accessible and interpretable for the LLMs, particularly in datasets with complex or diverse medical questions.

TABLE 5
Results of ablation experiments on five MedVQA datasets. "CIF" and "PM" represent the causal inference framework and the prompt module, respectively.

Parameters		Modules		VQA-RAD			SLAKE			PathVQA			PMC-VQA	ProbMed
7B	13B	CIF	PM	Open	Closed	Overall	Open	Closed	Overall	Open	Closed	Overall		
✓	-	✗	✗	69.3	84.2	78.2	78.9	81.5	79.9	32.0	70.1	51.1	36.0	53.0
✓	-	✗	✓	69.3	84.6	78.5	80.3	82.7	81.2	33.6	72.3	53.0	38.5	57.9
✓	-	✓	✗	73.7	86.4	81.4	84.8	86.5	85.5	38.3	81.7	60.1	43.6	66.3
✓	-	✓	✓	**74.3**	**87.1**	**82.0**	**90.1**	**90.4**	**90.2**	**40.4**	**87.9**	**64.2**	**44.0**	**69.4**
-	✓	✗	✗	70.4	84.6	78.9	79.8	81.7	80.6	32.6	71.0	51.9	36.6	54.0
-	✓	✗	✓	70.9	85.3	79.6	81.1	83.2	81.9	34.9	73.4	54.2	40.8	59.1
-	✓	✓	✗	73.7	87.1	81.8	85.9	87.5	86.5	38.9	85.6	62.3	44.2	67.2
-	✓	✓	✓	**76.0**	**87.9**	**83.1**	**90.5**	**91.8**	**91.0**	**41.4**	**91.5**	**66.5**	**46.7**	**70.7**

TABLE 6
Performance comparison of different vision and text encoders.

LB	VB	CIF+PM	PMC-VQA	ProbMed
BERT	ResNet-101	✗	16.3	31.2
	ResNet-101	✓	20.4	37.8
	MEVF	✗	20.9	35.5
	MEVF	✓	26.6	42.4
	CLIP ViT-B/16	✗	21.7	43.7
	CLIP ViT-B/16	✓	**30.4**	**51.0**
DeBERTa	ResNet-101	✗	25.1	38.9
	ResNet-101	✓	27.4	42.1
	MEVF	✗	30.5	40.3
	MEVF	✓	34.7	45.6
	CLIP ViT-B/16	✗	33.7	50.4
	CLIP ViT-B/16	✓	**39.2**	**57.2**
LLaMA-7B	ResNet-101	✗	23.4	41.7
	ResNet-101	✓	28.5	50.8
	MEVF	✗	30.2	44.1
	MEVF	✓	35.6	55.2
	CLIP ViT-B/16	✗	36.0	53.0
	CLIP ViT-B/16	✓	**44.0**	**69.4**

4.4.2 Impact Analysis of Encoders

Table 6 presents the performance comparison of different language backbones (LB), vision backbones (VB), and their combinations with the proposed CIF+PM framework on the PMC-VQA and ProbMed datasets. The results highlight the significant role of CIF+PM in improving the performance across different backbones.

Comparison Across Vision Backbones. Different vision backbones show varying levels of performance, with CLIP ViT-B/16 consistently outperforming ResNet-101 and MEVF. For instance, in the BERT setting without CIF+PM, CLIP achieves 21.7% and 43.7% on PMC-VQA and ProbMed, which is higher than ResNet-101 (16.3% and 31.2%) and MEVF (20.9% and 35.5%). This demonstrates that CLIP provides a stronger visual representation, which becomes even more effective when combined with CIF+PM. In the DeBERTa and LLaMA-7B settings, similar trends are observed, with CLIP + CIF+PM achieving the best results across both datasets, such as 39.2% on PMC-VQA and 57.2% on ProbMed for the DeBERTa, and 44.0% and 69.4% for LLaMA-7B.

Comparison Across Language Backbones. Language backbones also significantly impact performance. Among the three LBs, LLaMA-7B consistently achieves the best results, especially when combined with CIF+PM. For example, in the CLIP setting with CIF+PM, LLaMA-7B achieves the highest scores of 44.0% on PMC-VQA and 69.4% on ProbMed, outperforming DeBERTa (39.2% and 57.2%) and BERT (30.4% and 51.0%). These results suggest that LLaMA(7B), as a larger and more powerful language model, can better leverage the causal features extracted by CIF and the structured guidance provided by PM, particularly for complex datasets like ProbMed.

Effectiveness of CIF+PM. Across all combinations of LB and VB, the inclusion of CIF+PM consistently leads to substantial performance gains. For example, with the LLaMA-7B + CLIP backbone, CIF+PM improves the accuracy on PMC-VQA from 36.0% to 44.0% and on ProbMed from 53.0% to 69.4%. The results further highlight the complementary roles of CIF and PM. Without CIF+PM, even the best-performing backbones (e.g., LLaMA-7B + CLIP) achieve only 36.0% on PMC-VQA and 53.0% on ProbMed. However, the addition of CIF+PM leads to significant accuracy improvements, with increases of 8.0% on PMC-VQA and 16.4% on ProbMed. This underscores the effectiveness of CIF in mitigating the impact of confounders and aligning visual and textual elements under causal reasoning. Simultaneously, PM enhances the utilization of these causal features by providing structured, question-specific guidance, enabling the language model to focus on relevant context and generate accurate answers.

4.4.3 Parameter analysis

In MedVQA, we adopt the causal inference method to construct two modal mediators $\mathcal{M}_i$ and $\mathcal{M}_q$. To gain insight into the reasons for the performance improvement, we introduce an experiment that bypasses the Front-Door Adjustment (FDA) module by experimenting with extracted $\mathcal{M}_i$ and $\mathcal{M}_q$ directly. This is designed to investigate whether the performance improvement is due to confounding removal or the number of parameters introduced. Results in Table 7 show that for open-ended questions in the VQA-RAD dataset, using the FDA module improves accuracy by 3.4% compared to not using it. For closed questions, the increase is 1.4% and the overall performance improves by 2.2%. In the SLAKE dataset, the performances improve by 3.1%, 2.4%, and 2.8%, respectively. However, as shown in Table 5, the performance in VQA-RAD without CIF is 69.3%,

TABLE 7
Results of ablation experiments on the VQA-RAD dataset and SLAKE dataset. "FDA" represents the front-door adjustment module.

FDA	VQA-RAD			SLAKE		
	Open	Closed	Overall	Open	Closed	Overall
✗	70.9	85.7	79.8	87.0	88.0	87.4
✓	**74.3**	**87.1**	**82.0**	**90.1**	**90.4**	**90.2**

TABLE 8
Metric analysis experiments on the SLAKE dataset and PathVQA dataset.

Method	SLAKE		PathVQA	
	BLEU-1	F1	BLEU-1	F1
Med-Flamingo [52]	21.51	23.66	33.38	34.01
RadFM [53]	81.66	82.38	24.83	25.20
LLaVA-Med [7]	76.95	77.30	46.42	47.08
Uni-Med [54]	82.12	83.07	58.07	58.74
Ours	**85.40**	**85.25**	**63.93**	**62.72**

84.6%, and 78.5%. After using CIF, even without using the FDA module, there is a slight performance improvement of 1.6%, 1.1%, and 1.3%, due to the role of the mediators. As shown in Fig. 4, although the process of building mediators is not a complete causal inference process, it is essentially a feature fusion mechanism. This means that $\mathcal{M}_i$ and $\mathcal{M}_q$ are more information-rich than the original features, resulting in a slight performance improvement. However, with the use of FDA, the performance improvements reached 4.0%, 2.5%, and 3.5%, respectively, far exceeding the effects of only using mediators. This clearly shows that the significant improvement in performance is almost entirely due to the causal inference process and not just the introduction of the number of parameters. At the same time, this highlights the need to ensure the integrity of the CIF module.

4.5 Metric Analysis

Table 8 shows the performance comparison of different methods on the SLAKE and PathVQA datasets using BLEU-1 and F1 metrics. Our method achieves the highest scores across both datasets, with BLEU-1 and F1 scores of 91.40 and 85.25 on SLAKE, and 66.93 and 62.72 on PathVQA, respectively. Compared to the strongest baseline Uni-Med, our method improves BLEU-1 by 3.28 and 5.86 points and F1 by 2.18 and 3.98 points on SLAKE and PathVQA, respectively. These results demonstrate the superior ability of our approach to generate precise and semantically aligned answers. The causal inference framework (CIF) effectively mitigates confounding effects and aligns visual and textual features under causal relationships, while the prompt module (PM) enhances the model's understanding of complex medical questions by providing structured guidance.

4.6 Qualitative Analysis

Fig. 5 shows the significant changes in the model's attention distribution and corresponding answer accuracy before and after applying the CIF module across various medical imaging modalities, including lung (X-ray/CT), brain (MRI), and abdomen (CT) images. On lung images, when answering the question "Where is the pleural effusion?", the model without CIF incorrectly focused on the lower right lung instead of the true lesion area in the lower left lung. This error is caused by confounding effects, which misled the model to associate frequent statistical correlations with the answer. After introducing CIF, the model correctly attended to the pleural effusion region in the lower left lung and provided the correct answer, demonstrating CIF's ability to eliminate spurious correlations and guide the model to identify causally relevant regions based on causal reasoning. On brain MRI images, CIF effectively mitigates the influence of confounding regions in complex brain imaging tasks, significantly improving the model's focus on causally relevant areas. Similarly, on abdominal CT images, when asked "What is the largest organ in the picture?", the model without CIF mistakenly focused on the irrelevant organ and produced an incorrect answer. In contrast, the model with CIF accurately generated the correct answer, demonstrating CIF's capability to separate causally relevant features from irrelevant ones, even in complex multi-organ imaging scenarios.

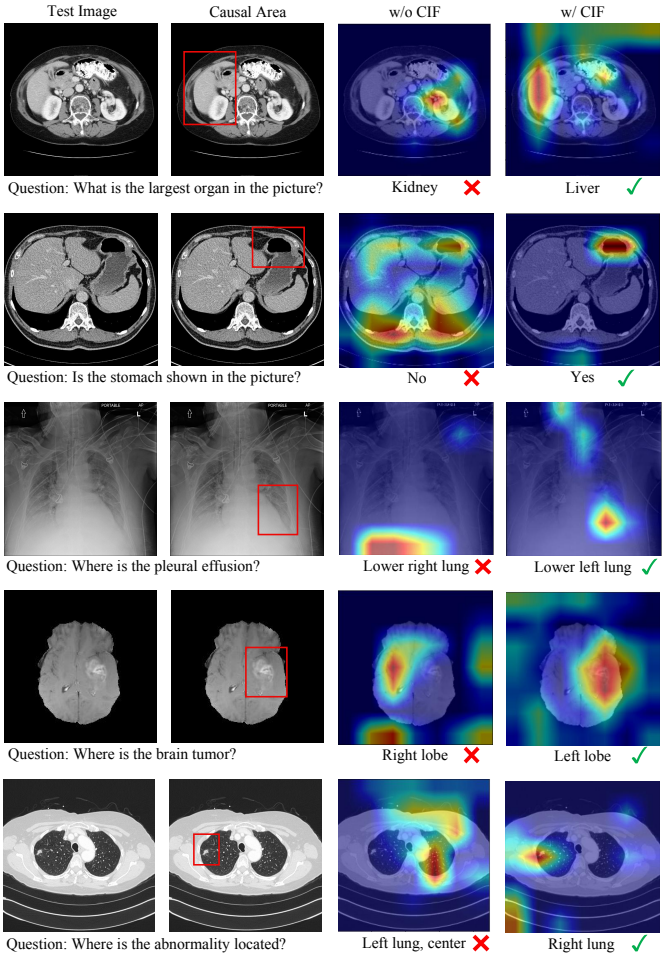

Fig. 5. Visualization Results of CIF on Lung (X-ray, CT), Brain (MRI), and Abdomen (CT) Imaging.

Overall, without CIF, the model is often misled by confounding effects, dispersing its attention to non-causal regions and producing incorrect answers. With CIF, the model's attention is effectively concentrated on regions directly relevant to the question, resulting in significantly

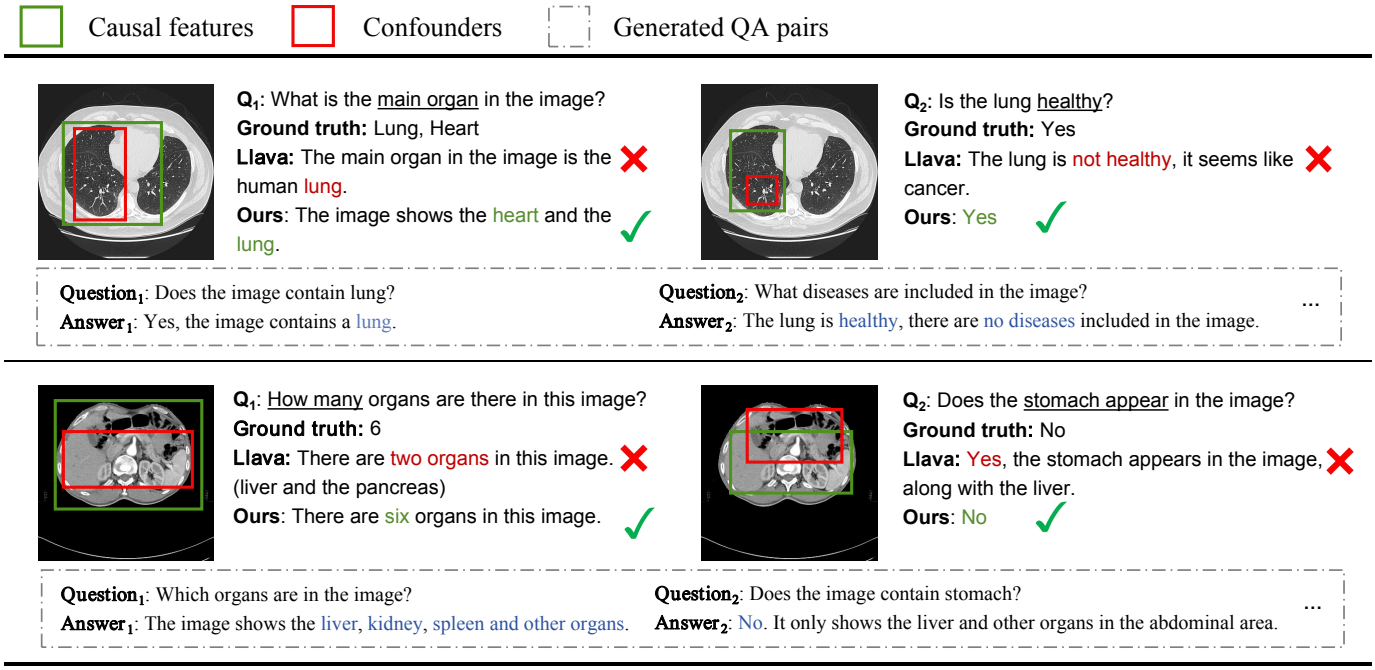

Fig. 6. Qualitative results on SLAKE. Combined with the causal inference and prompt modules, our approach performs well in MedVQA. The blue font represents the part of the prompt text that guides the correct answer.

improved answer accuracy. These results validate CIF's critical role in mitigating the influence of spurious correlations, enabling the model to focus on causally relevant regions, and strengthening the causal alignment between visual and textual modalities.

Fig. 6 shows the qualitative analysis of our proposed method. We select two images, each corresponding to two questions. In both cases, there is a situation where the region of confounder that leads the model to make an incorrect prediction, is actually the real cause of another question. In the first image, Llava [55] ignores the presence of the heart and misdiagnoses the healthy image as cancer. In the second image, Llava has trouble recognizing organs. For different questions with each image, CIF captures different confounding factors. By eliminating spurious associations caused by relative confounders, CIF guides the model to provide accurate answers. In addition, some of the QA pairs generated by PM include the correct answers. By controlling the form of the generated QA pairs, PM is broadly applicable and provides useful information for both open and closed questions. These examples highlight the critical role of causal inference and prompt strategy in MedVQA.

5 Discussion

5.1 Causal inference

In our work, we leveraged the front-door adjustment (FDA) method from causal inference to address confounding effects in the MedVQA task. As shown in Fig. 2, the FDA approach introduces two mediating variables, $\mathcal{M}_i$ and $\mathcal{M}_q$, which effectively cut off the backdoor paths. This adjustment aims to eliminate the influence of confounders and allows for a more accurate estimation of the causal effect.We implemented the FDA in MedVQA, by intervening in the variables I and Q to block the backdoor paths. This approach is well-established in causal inference and has demonstrated success in various applications. To solidify our research's theoretical foundation, we simplified the probability formula in Eq.1 through mathematical analysis.

Our investigation delved into the mathematical principles underlying causal inference, followed by extensive experiments and analyses. The critical aspect of applying causal inference lies in realizing the probability formulas derived from theoretical foundations, bridging theory and practice. This process necessitates translating theoretical formulas into practical sub-networks. After numerous attempts, we constructed mediating variables based on the attention mechanism (as detailed in Fig 4). By utilizing the FDA formula, we decomposed the causal effect into the product of the distribution of the mediating variable and the distribution of the target variable, enabling a more precise estimation of the causal effect. This method underscores the potential of causal inference techniques in enhancing the reliability and accuracy of outcomes in MedVQA tasks.

5.2 Prompt module

In our approach, we employed prompts as auxiliary information to address the alignment challenges between different modalities. This integration allows large language models (LLMs) to leverage causal features more effectively. While causal inference frameworks (CIF) can eliminate confounders, the inherent complexity of LLMs can sometimes hinder their ability to fully grasp the specific context and questions. As a result, the causal features may not be optimally utilized.

The introduction of prompt modules (PM) offers a solution by providing more targeted information, enhancing the model's flexibility in understanding and responding to

questions. The prompts serve as a bridge, facilitating better comprehension and alignment within the LLMs. We observed that the combination of CIF and PM yielded superior performance, which can be attributed to their complementary roles. CIF mitigates the impact of confounders, ensuring a clearer causal pathway, while PM supplies the necessary contextual information, optimizing the LLM's interpretative and response capabilities. In conclusion, this synergy between causal inference and prompt modules underscores a significant advancement in MedVQA tasks.

5.3 Limitation

Despite the promising results achieved with our current approach, there are notable limitations that warrant discussion. Our method of constructing mediating variables, although effective, may still be limited in its ability to fully eliminate confounding effects. The complexity and variability inherent in medical visual question answering tasks mean that there may be residual confounders that our current model does not completely account for. This limitation underscores the need for continuous refinement and improvement of our mediating variable construction techniques. Furthermore, while our approach has successfully leveraged causal inference principles to enhance model performance, there remains an ongoing challenge in quantifying the impact of eliminating confounders. Future work will focus on calculating the causal effect to more precisely measure the extent to which confounding influences have been mitigated.

6 Conclusion

In this work, we propose a novel causal inference framework to learn the causal structure of multi-modal medical information from the perspective of causal representation. We emphasize the correlation of confounders, reduce their impact by employing multi-variate resampling front-door adjustments, and finally achieve true causal associations between MedVQA data. In addition, we design a prompt module to help the LLMs understand the context of the questions and the visual scene. It allows the model to better generalize to multi-modal medical data while reducing the deployment cost of the model. By combining the two with pre-trained visual and language backbones, we have significantly improved the accuracy of MedVQA, which is expected to promote deep learning research and the application of multi-modal medical information.

References

[1] S. Lu, Y. Ding, M. Liu, Z. Yin, L. Yin, and W. Zheng, "Multiscale feature extraction and fusion of image and text in vqa," *International Journal of Computational Intelligence Systems*, vol. 16, 2023.

[2] J. G. et al., "From images to textual prompts: Zero-shot visual question answering with frozen large language models," in *Proceedings of the IEEE/CVF conference on computer vision and pattern recognition*, 2023, pp. 10 867–10 877.

[3] A. M. H. Tiong, J. Li, B. Li, S. Savarese, and S. C. Hoi, "Plug-and-play vqa: Zero-shot vqa by conjoining large pretrained models with zero training," *arXiv preprint arXiv:2210.08773*, 2022.

[4] A. B. Abacha, S. Gayen, J. J. Lau, S. Rajaraman, and D. Demner-Fushman, "Nlm at imageclef 2018 visual question answering in the medical domain." in *CLEF (working notes)*, 2018, pp. 1–10.

[5] N. W. et al., "Chest x-ray image classification: A causal perspective," in *International Conference on Medical Image Computing and Computer-Assisted Intervention*. Springer, 2023, pp. 25–35.

[6] W. Nie, C. Zhang, D. Song, Y. Bai, K. Xie, and A. Liu, "Instrumental variable learning for chest x-ray classification," in *2023 IEEE International Conference on Systems, Man, and Cybernetics (SMC)*. IEEE, 2023, pp. 4506–4512.

[7] C. Li, C. Wong, S. Zhang, N. Usuyama, H. Liu, J. Yang, T. Naumann, H. Poon, and J. Gao, "Llava-med: Training a large language-and-vision assistant for biomedicine in one day," *Advances in Neural Information Processing Systems*, vol. 36, 2024.

[8] C. Wu, W. Lin, X. Zhang, Y. Zhang, W. Xie, and Y. Wang, "Pmc-llama: toward building open-source language models for medicine," *Journal of the American Medical Informatics Association*, p. ocae045, 2024.

[9] X. Z. et al., "Pmc-vqa: Visual instruction tuning for medical visual question answering," *arXiv preprint arXiv:2305.10415*, 2023.

[10] L.-M. Zhan, B. Liu, L. Fan, J. Chen, and X.-M. Wu, "Medical visual question answering via conditional reasoning," in *Proceedings of the 28th ACM International Conference on Multimedia*, 2020, pp. 2345–2354.

[11] B. D. Nguyen, T.-T. Do, B. X. Nguyen, T. Do, E. Tjiputra, and Q. D. Tran, "Overcoming data limitation in medical visual question answering," in *Medical Image Computing and Computer Assisted Intervention–MICCAI 2019*. Springer, 2019, pp. 522–530.

[12] L. W. et al., "Pmc-clip: Contrastive language-image pre-training using biomedical documents," in *International Conference on Medical Image Computing and Computer-Assisted Intervention*. Springer, 2023, pp. 525–536.

[13] J. Pearl, "Causal inference in statistics: An overview," *Statistics Surveys*, vol. 3, pp. 96–146, 2009.

[14] K. Z. et al., "gcastle: A python toolbox for causal discovery," *arXiv preprint arXiv:2111.15155*, 2021.

[15] J. e. a. Yuan, "Auto iv: Counterfactual prediction via automatic instrumental variable decomposition," *ACM Transactions on Knowledge Discovery from Data (TKDD)*, vol. 16, no. 4, pp. 1–20, 2022.

[16] X. Yang, S. Wang, J. Dong, J. Dong, M. Wang, and T.-S. Chua, "Video moment retrieval with cross-modal neural architecture search," *IEEE Transactions on Image Processing*, vol. 31, pp. 1204–1216, 2022.

[17] S. Rajaraman and S. Antani, "Training deep learning algorithms with weakly labeled pneumonia chest x-ray data for covid-19 detection," *MedRxiv*, 2020.

[18] X. Wang, Y. Peng, L. Lu, Z. Lu, M. Bagheri, and R. M. Summers, "Chestx-ray8: Hospital-scale chest x-ray database and benchmarks on weakly-supervised classification and localization of common thorax diseases," in *Proceedings of the IEEE conference on computer vision and pattern recognition*, 2017, pp. 2097–2106.

[19] Y. Zhang, B. Kang, B. Hooi, S. Yan, and J. Feng, "Deep long-tailed learning: A survey," *IEEE Transactions on Pattern Analysis and Machine Intelligence*, vol. 45, no. 9, pp. 10 795–10 816, 2023.

[20] K. Li, J. Li, D. Guo, X. Yang, and M. Wang, "Transformer-based visual grounding with cross-modality interaction," *ACM Trans. Multimedia Comput. Commun. Appl.*, vol. 19, no. 6, May 2023.

[21] D. Zhang, H. Zhang, J. Tang, X.-S. Hua, and Q. Sun, "Causal intervention for weakly-supervised semantic segmentation," *Advances in Neural Information Processing Systems*, vol. 33, pp. 655–666, 2020.

[22] E. Bareinboim and J. Pearl, "Controlling selection bias in causal inference," in *Artificial Intelligence and Statistics*. PMLR, 2012, pp. 100–108.

[23] T. Wang, J. Huang, H. Zhang, and Q. Sun, "Visual commonsense r-cnn," *2020 IEEE/CVF Conference on Computer Vision and Pattern Recognition (CVPR)*, pp. 10 757–10 767, 2020.

[24] X. Yang, H. Zhang, and J. Cai, "Deconfounded image captioning: A causal retrospect," *IEEE Transactions on Pattern Analysis and Machine Intelligence*, vol. 45, no. 11, pp. 12 996–13 010, 2021.

[25] J. Li, B. Wu, X. Sun, and Y. Wang, "Causal hidden markov model for time series disease forecasting," *2021 IEEE/CVF Conference on Computer Vision and Pattern Recognition (CVPR)*, pp. 12 100–12 109, 2021.

[26] X. Yang, F. Feng, W. Ji, M. Wang, and T.-S. Chua, "Deconfounded video moment retrieval with causal intervention," in *Proceedings of the 44th International ACM SIGIR Conference on Research and Development in Information Retrieval*, ser. SIGIR '21. New York, NY, USA: Association for Computing Machinery, 2021, p. 1–10.

[27] Z. Yue, H. Zhang, Q. Sun, and X.-S. Hua, "Interventional few-shot learning," *Advances in neural information processing systems*, vol. 33, pp. 2734–2746, 2020.

[28] X. Yang, H. Zhang, G. Qi, and J. Cai, "Causal attention for vision-language tasks," in *Proceedings of the IEEE/CVF conference on computer vision and pattern recognition*, 2021, pp. 9847–9857.

[29] C. Zang, H. Wang, M. Pei, and W. Liang, "Discovering the real association: Multimodal causal reasoning in video question answering," *2023 IEEE/CVF Conference on Computer Vision and Pattern Recognition (CVPR)*, pp. 19 027–19 036, 2023.

[30] J. J. Lau, S. Gayen, A. Ben Abacha, and D. Demner-Fushman, "A dataset of clinically generated visual questions and answers about radiology images," *Scientific data*, vol. 5, no. 1, pp. 1–10, 2018.

[31] Y. Peng, F. Liu, and M. P. Rosen, "Umass at imageclef medical visual question answering (med-vqa) 2018 task." in *CLEF (working notes)*, 2018, pp. 1–9.

[32] Y. Zhou, X. Kang, and F. Ren, "Employing inception-resnet-v2 and bi-lstm for medical domain visual question answering." in *CLEF (working notes)*, 2018, pp. 1–11.

[33] K. Simonyan and A. Zisserman, "Very deep convolutional networks for large-scale image recognition," *CoRR*, vol. abs/1409.1556, 2014.

[34] K. He, X. Zhang, S. Ren, and J. Sun, "Deep residual learning for image recognition," *2016 IEEE Conference on Computer Vision and Pattern Recognition (CVPR)*, pp. 770–778, 2015.

[35] J. Masci, U. Meier, D. Cireşan, and J. Schmidhuber, "Stacked convolutional auto-encoders for hierarchical feature extraction," in *Artificial Neural Networks and Machine Learning–ICANN 2011*. Springer, 2011, pp. 52–59.

[36] R. Vuorio, S.-H. Sun, H. Hu, and J. J. Lim, "Multimodal model-agnostic meta-learning via task-aware modulation," *Advances in neural information processing systems*, vol. 32, 2019.

[37] B. Liu, L.-M. Zhan, and X.-M. Wu, "Contrastive pre-training and representation distillation for medical visual question answering based on radiology images," in *Medical Image Computing and Computer Assisted Intervention–MICCAI 2021*. Springer, 2021, pp. 210–220.

[38] C. Z. et al., "Multi-modal masked autoencoders for medical vision-and-language pre-training," in *International Conference on Medical Image Computing and Computer-Assisted Intervention*. Springer, 2022, pp. 679–689.

[39] X. Huang and H. Gong, "A dual-attention learning network with word and sentence embedding for medical visual question answering," *IEEE Transactions on Medical Imaging*, 2023.

[40] C. Zhan, P. Peng, H. Zhang, H. Sun, C. Shang, T. Chen, H. Wang, G. Wang, and H. Wang, "Debiasing medical visual question answering via counterfactual training," in *International Conference on Medical Image Computing and Computer-Assisted Intervention*. Springer, 2023, pp. 382–393.

[41] S. Ye, U. Naseem, M. Meng, D. Feng, and J. Kim, "A causal approach to mitigate modality preference bias in medical visual question answering," in *Proceedings of the First International Workshop on Vision-Language Models for Biomedical Applications*, 2024, pp. 13–17.

[42] L. Cai, H. Fang, N. Xu, and B. Ren, "Counterfactual causal-effect intervention for interpretable medical visual question answering," *IEEE Transactions on Medical Imaging*, 2024.

[43] Y. Liu, G. Li, and L. Lin, "Cross-modal causal relational reasoning for event-level visual question answering," *IEEE Transactions on Pattern Analysis and Machine Intelligence*, vol. 45, pp. 11 624–11 641, 2022.

[44] X. K. et al., "Show, attend and tell: Neural image caption generation with visual attention," in *International conference on machine learning*. PMLR, 2015, pp. 2048–2057.

[45] R. A. et al., "Learning transferable visual models from natural language supervision," in *Proceedings of the 38th International Conference on Machine Learning*, ser. Proceedings of Machine Learning Research, M. Meila and T. Zhang, Eds., vol. 139. PMLR, 18–24 Jul 2021, pp. 8748–8763.

[46] B. Liu, L.-M. Zhan, L. Xu, L. Ma, Y. Yang, and X.-M. Wu, "Slake: A semantically-labeled knowledge-enhanced dataset for medical visual question answering," in *2021 IEEE 18th International Symposium on Biomedical Imaging (ISBI)*. IEEE, 2021, pp. 1650–1654.

[47] X. He, Y. Zhang, L. Mou, E. P. Xing, and P. Xie, "Pathvqa: 30000+ questions for medical visual question answering," *ArXiv*, vol. abs/2003.10286, 2020.

[48] T. Van Sonsbeek, M. M. Derakhshani, I. Najdenkoska, C. G. Snoek, and M. Worring, "Open-ended medical visual question answering through prefix tuning of language models," in *International Conference on Medical Image Computing and Computer-Assisted Intervention*. Springer, 2023, pp. 726–736.

[49] P. Li, G. Liu, L. Tan, J. Liao, and S. Zhong, "Self-supervised vision-language pretraining for medial visual question answering," in *2023 IEEE 20th International Symposium on Biomedical Imaging (ISBI)*. IEEE, 2023, pp. 1–5.

[50] X. Zhang, C. Wu, Z. Zhao, W. Lin, Y. Zhang, Y. Wang, and W. Xie, "Pmc-vqa: Visual instruction tuning for medical visual question answering," *arXiv preprint arXiv:2305.10415*, 2023.

[51] Q. Yan, X. He, X. Yue, and X. E. Wang, "Worse than random? an embarrassingly simple probing evaluation of large multimodal models in medical vqa," *arXiv preprint arXiv:2405.20421*, 2024.

[52] M. Moor, Q. Huang, S. Wu, M. Yasunaga, Y. Dalmia, J. Leskovec, C. Zakka, E. P. Reis, and P. Rajpurkar, "Med-flamingo: a multimodal medical few-shot learner," in *Machine Learning for Health (ML4H)*. PMLR, 2023, pp. 353–367.

[53] C. Wu, X. Zhang, Y. Zhang, Y. Wang, and W. Xie, "Towards generalist foundation model for radiology," *arXiv preprint arXiv:2308.02463*, 2023.

[54] X. Zhu, Y. Hu, F. Mo, M. Li, and J. Wu, "Uni-med: A unified medical generalist foundation model for multi-task learning via connector-moe," *arXiv preprint arXiv:2409.17508*, 2024.

[55] H. Liu, C. Li, Q. Wu, and Y. J. Lee, "Visual instruction tuning," in *Advances in Neural Information Processing Systems*, vol. 36. Curran Associates, Inc., 2023, pp. 34 892–34 916.